High-Energy Physics Laboratory
W. W. Hansen Laboratories of Physics
STANFORD UNIVERSITY
STANFORD, CALIFORNIA

ELECTRON-PROTON COINCIDENCES

IN

INELASTIC ELECTRON DEUTERON SCATTERING

By

M. G. CROISSIAUX

Technical Report
Linear Electron Accelerator Project
Contract N6onr-25116

HEPL Report No. 264
June 1962

High-Energy Physics Laboratory
W. W. HANSEN LABORATORIES OF PHYSICS
Stanford University
Stanford, California

and

Centre de Recherches Nucléaires
Strasbourg, France

ACKNOWLEDGEMENTS

I wish to thank Professor R. Hofstadter for suggesting this experiment and for many helpful discussions. I am also indebted to many people of the laboratory who assisted me during the different stages of this work

Note: I ask the indulgence of the readers, if they find any grammatical errors.

CONTENTS

Page

ACKNOWLEDGEMENTS . . . . . .

LIST OF TABLES . . . . . .

LIST OF FIGURES. . . . . .

INTRODUCTION. . . . . .

Chapter

I. EXPERIMENTAL APPARATUS . . . . . .

A. Introduction . . . . . .

B. Electron Counter . . . . . .

C. Proton Multichannel and Electronic Circuits . .

D. Target . . . . . .

II. EXPERIMENTAL METHOD . . . . . .

A. Slits Problem . . . . . .

B. Interpretation. . . . . .

III. EXPERIMENTAL PROCEDURE . . . . . .

IV. RESULTS . . . . . .

V. INTERPRETATION OF THE RESULTS . . . . . .

A. Introduction . . . . . .

B. Connections Between our Measurement and the Durand's Formula . . . . . .

C. Comparison of our Result with the Theory . . .

LIST OF TABLES

Table Page

I. Typical Schedule of Counts Obtained with the 10-Channel Ladder. . . . . .

LIST OF FIGURES

Figure — Page

1. Block diagram of electronics used for research of electron-proton coincidences. . . . . .

2. Target arrangement. . . . . .

3. Pulse height distribution in the electron counter . .

4. Single electron peak with a liquid hydrogen target. For coincidences, the dispersion slits count pulses coming in dE'_e indicated by the width of a step. To measure the total coincidences number with H^2, we set the magnet current on each of the three steps mentioned in the Figure. The stainless steel background is small . . . . . .

5. Single protor peak with a liquid H^2 target. One can see that the background of the stainless steel is not negligible . . . . . .

6. Slits problem—counts versus the slits opening—the theoretical positions correspond to a point target. In the vertical plane, the read-out 370 corresponds at 4". In the horizontal plane, the read-out 276 corresponds at 1" . . . . . .

7. Slits problem—the curves of Figure 6 are explained by the thickness of the target—a coincidence can happen in A as well as in O or B. . . . . .

8. Example of the pulse height distribution on one proton counter. The background is small and one get easily a narrow peak . . . . . .

9. Measurement of the efficiency of the 10 channels of the proton detection by counting the coincidence peak (with H^2 target) (analogous to the peak of Figure 5b) on each crystal by moving the current setting of the 72" magnet . . . . . .

10. Coincidence spectrum with D^2 target. The H^2 peak is for comparison of the position of the peak. The shift between the two maxima is due to the binding energy of the deuteron. The big accidental coincidence counting rate is due to the large τ necessary to get all coincidences according to the large time of flight difference of protons in the 72" magnet . .

Figure Page

11. Radiative correction problem. The correction to be applied in coincidence depends on the cut position E and P in the single electron and proton peak. The curves shown are an example with an H^2 target. . . .

12. Proton momentum at the expected peak of the e-p coincidences versus the angle of the proton magnet. (The 0° direction is the q direction, according to Durand's paper.) . . . . . .

13. Calculated theoretical cross section from Durand's formula in the lab system . . . . . .

14. Cutting out scheme of the entrance slits in the proton magnet to take into account the angular distribution of protons . . . . . .

INTRODUCTION

The presence of two magnetic spectrometers in the "end station" of the Stanford linear accelerator has opened a new field of research in electron scattering problems. Obviously, one can take data independently with these two magnets, but more than that, one has the possibility of detecting two products of the reaction in coincidence, for instance, among other cases, the scattered electron and the recoiling nucleus, or one of the nucleons after the break up of the nucleus.

We can think of many experiments where this method would be useful. We have begun to study the problem of e-p coincidences in deuterium with the detection of relatively energetic protons (above 50 Mev). This experiment can give much information about different questions, for instance: one can compare the form factors of the proton in a bound state to those of a free proton; one can have more details on the neutron form factors and get some idea about the final state interaction and the meson exchange current.

We have to say also that the neutron form factors can be obtained more easily from the measurement of the e-n coincidence (with the detection of high-energy neutron) or the coincidence e-p (with low-energy proton, less than 10 Mev).

In the experiment discussed here, we try to find a value for the proton form factors in a bound state and see if they are equal to those obtained for a free proton. In fact, in all theories, they are assumed to be equal, but it seems to be useful to check it and also to see if there is no meson exchange effect which would change the values of these

form factors.*

In Chapter I, we give details on the experimental apparatus; in Chapter II we show some problems connected with this experiment; Chapter III explains the experimental procedure and how to get the data; Chapter IV gives the results; and, in Chapter V we perform the calculations on the theoretical formula in order to interpret the results and give the conclusion of the experiment in Chapter VI.

*Since the time this report was prepared and typed, new runs have been performed on the experiment with some new experimental details. To the first order the improvements left unchanged the results. Therefore, it is thought that this report can still be useful.

CHAPTER I

EXPERIMENTAL APPARATUS

A. Introduction

To count the e-p coincidences, we use an electron counter in the 36" spectrometer and a multichannel system in the 72" spectrometer to detect the protons. All the pulses are sent directly from the end station to the counting room where all the electronic equipment is installed.

We could use also the 36" magnet to detect the protons and the 72" for electron counting, but it would be less convenient in this case for several reasons:

1) With the 36", one can deflect protons of only energy less than 125 Mev; this limits the ability to use incident high energy beam and/or backward angle for electrons.
2) To adjust the delay between the electron and proton pulses we have to do a delay curve which is more convenient to do with one variable delay box placed on the electron side. This requires that the electron pulses come earlier than the proton pulses. Because of the time of flight of electrons and protons through the magnets, it is often easier to use the 36" spectrometer for the electron detection.

Although in this experiment it is not necessary to count single pulses from each counter, but only coincidences, we believe it safe to do so. In this way, we can compare the counting rate and cross sections

from the single and coincidence pulses.

The general scheme of the electronics is shown in Figure 1.

B. Electron Counter

The electron counter is a Cerenkov counter filled with the fluorochemical liquid (refraction index n = 1.276), 8 inches long. The entrance face has a diameter of 3.5 inches. A 5" photomultiplier RCA 7046 is looking at the counter and sends two pulses in the counting room. The fast negative pulses from the anode are used for coincidence.

The fast positive pulse from the last-dynode is used to count the single counts and look at the pulse height spectrum of the counter.

Table Ia

Cable number	End station	Between end station and counting room	Counting room
HV.	633	44 on bay x 10	to distribution panel
Anode	634	177 x 29	25
Dynode	635	66 x 10	to bay x 4 (position written 36")

The anode pulses come by the cable no. 25 to a variable delay box (minimum delay 13 feet 2 inches - maximum + 10 feet of RG 63/U), then to the splitting circuit and finally to the 10 inputs of the coincidence circuits.

The dynode pulse is sent on scaler A. The cable must be matched at 125 ohms.

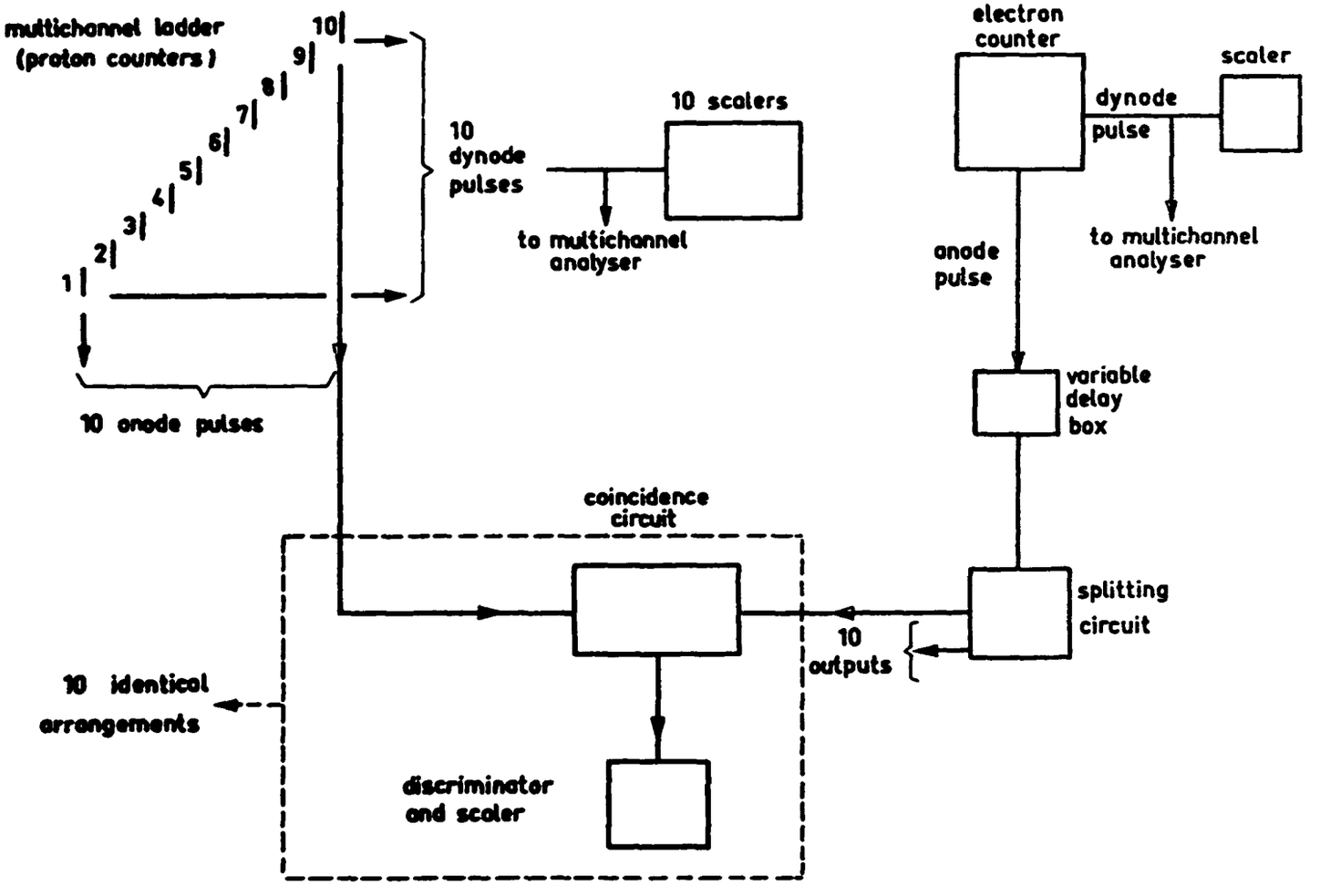
multichannel ladder
(proton counters)
10
9
8
7
6
5
4
3
2
1
10 dynode pulses
10 scalers
to multichannel analyser
10 anode pulses
electron counter
scaler
dynode pulse
to multichannel analyser
anode pulse
variable delay box
coincidence circuit
splitting circuit
10 outputs
10 identical arrangements
discriminator and scaler

Fig. 1

The voltage for the photomultiplier was +2890 volts.

With the exit horizontal slits at 1.5", we can work with exit vertical slits as big as 3" maximum if the magnet properties are good. Until now, we opened them at 1.5", which corresponds to more than 1% dispersion of the 36".

C. Proton Multichannel and Electronic Circuits

All details are discussed in the High-Energy Physics Laboratory Internal Memorandum, HEPL-247, Stanford University, Stanford, California.

D. Target

By using a solid target (CH^2 and CD^2), we can have good geometry and a target as thin as we wish. In fact, we always preferred to use a liquid target to avoid the electro- or photoproduction by the C^{12} nuclei. (With a CH^2 target, we measured about 60% of the single protons coming from C^{12} with these conditions, and a CD^2 target, the protons from D^2 in the inelastic peak would represent only 10% of the counted protons.)

The only liquid target available was a cigar-shaped target, 7.5" long and 1" in diameter. We placed it in the position shown in Figure 2. The axis of the target was at 75° of the beam axis.

For the reason discussed in Chapter II, we intend to use later a flat thin liquid target ($\frac{5"}{16}$ thick). It will always be perpendicular to the beam and there will be no frame on any side in such a way that

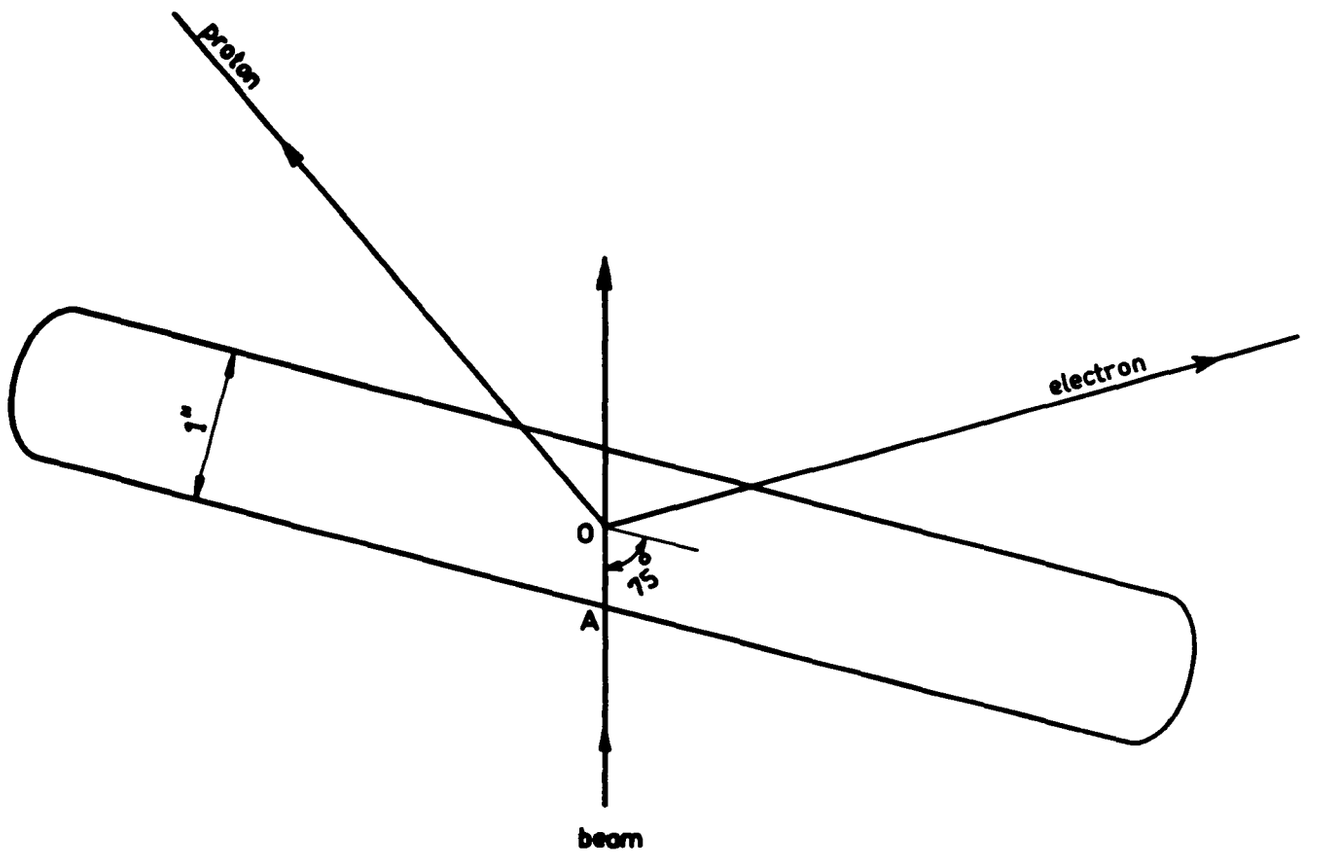

Fig. 2

one can detect protons up to 90° in the laboratory system and electrons up to 135° in the same system.*

*In January, 1962, the new target described above was tried and used successfully.

CHAPTER II

EXPERIMENTAL METHOD

Unless noted, we have always worked with an incident electron beam of E_e = 500 Mev and have detected the scattered electrons at $\theta_e = 75°$ with the 36" magnet. The recoiling protons are scattered at $\varphi_p = 40°$ 23 minutes from the beam axis with a H^2 target.

Before looking at the coincidence in deuterium, it is good to check that we get the right cross-section by the electron-proton coincidences with a hydrogen target. We must get the same cross-section with such a target from the counting of: a) the single electrons; b) the single protons; and, c) the coincidence electron-proton. (Point [c] is also a check for all the electronic apparatus.

a) The measurement of the cross section by counting the single electrons is usual. We show in Figure 3 the electron pulse height distribution. With the discrimination level shown in the figure, we get the electron peak of Figure 4. The background due to the stainless steel frame of the target is small (about 3%). From the peak it is easy to find the cross section from counting the single electrons.

$$\frac{d\sigma}{d\Omega_e} = \frac{n}{N_T N_e d\Omega_e} \qquad (1)$$

n = number of counts in the peak

N_T = number of protons in the target (in area of 1 cm^2)

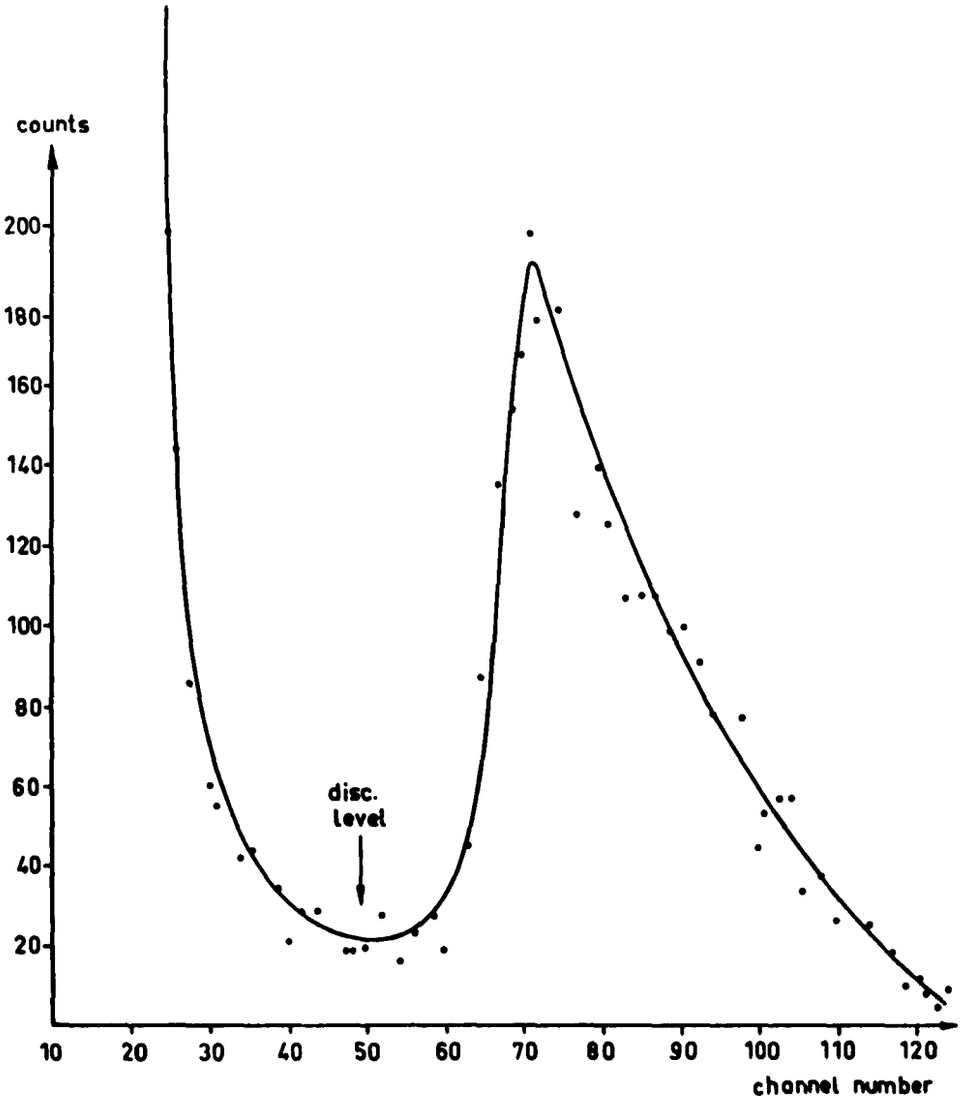
counts
200
180
160
140
120
100
80
60
40
20
disc.
level
10
20
30
40
50
60
70
80
90
100
110
120
channel number

Fig. 3

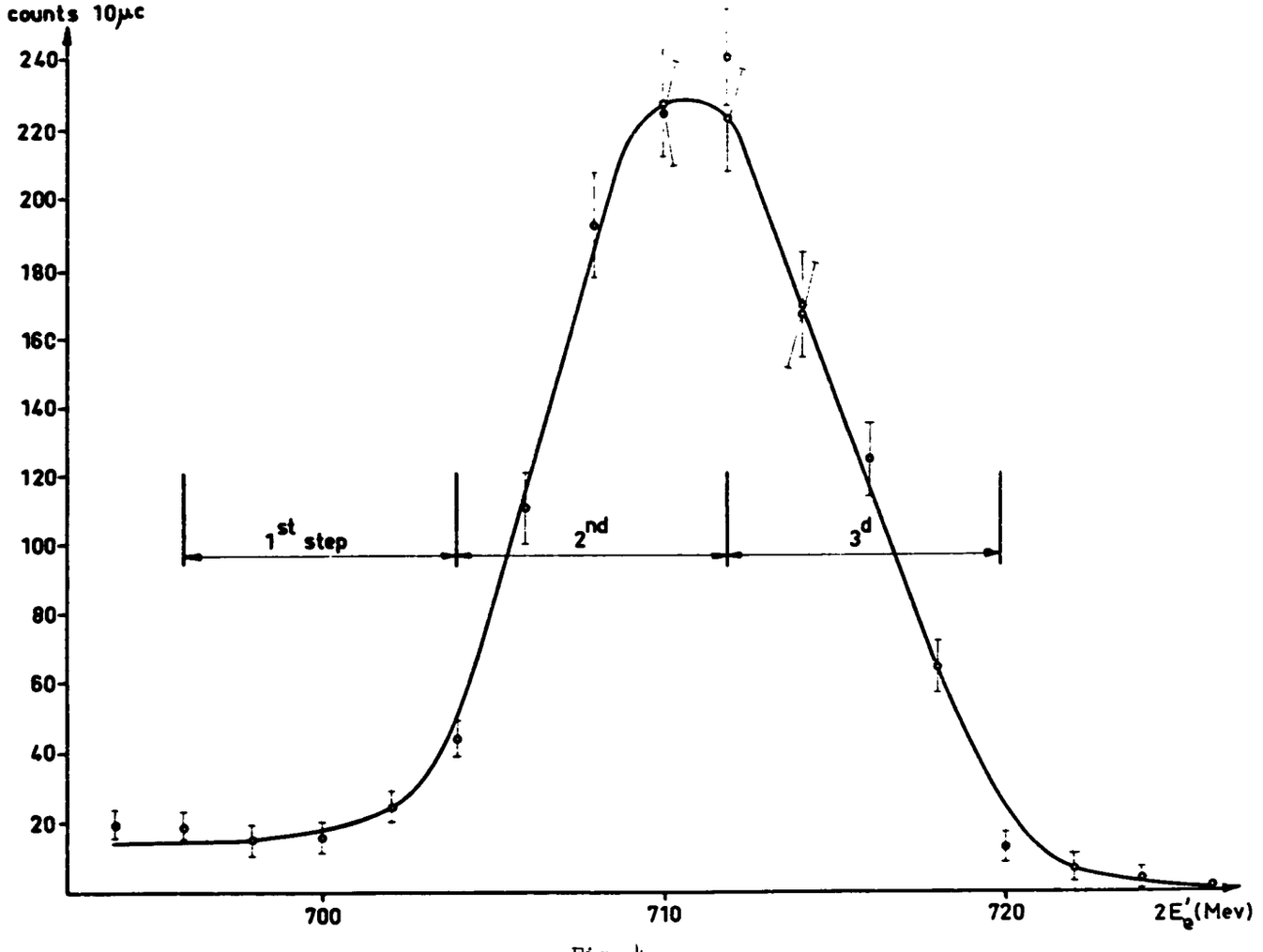
counts 10μc
240
220
200
180
160
140
120
100
80
60
40
20
1st step
2nd
3d
700
710
720
2E'e(Mev)

Fig. 4

N_e = number of electrons

$d\Omega_e$ = entrance solid angle of the spectrometer

n depends also upon the dispersion of the magnet (exit slits) and contains the radiative correction.

b) In this case, the electroproduction or photoproduction of protons from the stainless steel is not negligible (Figure 5a) and we have to do the subtraction. It may be hard to accurately evaluate this background if we do not have an empty target to measure it.

The entrance solid angle to be accounted for in the cross section formula (1) is not the real solid angle from proton detection, but the equivalent solid angle for electrons which one can take out of the angular kinematic relation between the electrons and recoil protons.

c) The cross section measurement from e-p coincidences (with H^2 target) requires some attention on the problem of the slits.

A. Slits Problem

They must be small enough so that the particles going through the magnets are in regions in which the magnetic focusing properties are satisfactory.

Case a) Counting of Single Electrons

E'_e = 359 Mev

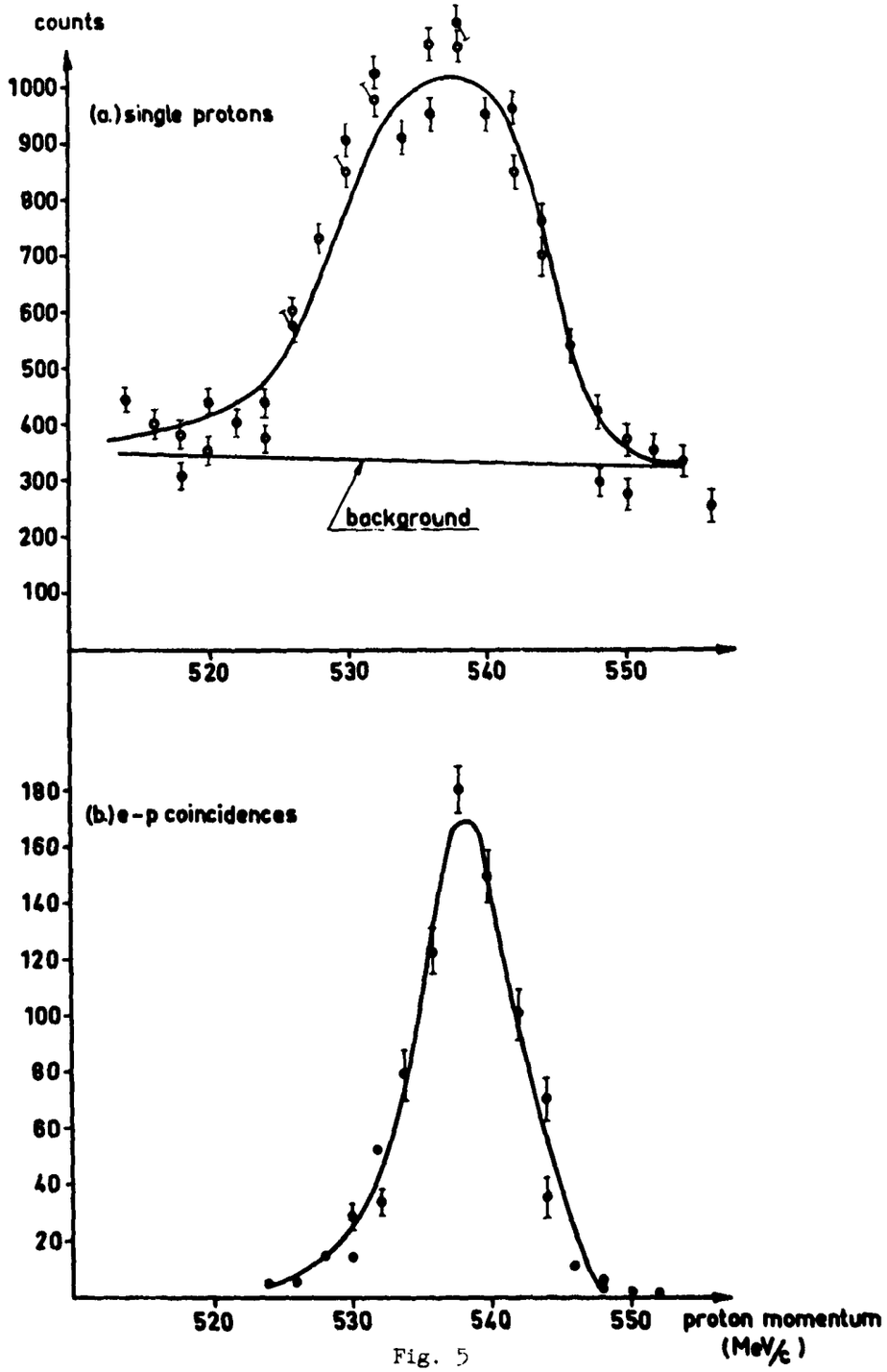
counts
1000
900
800
700
600
500
400
300
200
100
(a.) single protons
background
520
530
540
550
180
160
140
120
100
80
60
40
20
(b.) e-p coincidences
520
530
540
550
proton momentum
(MeV/c)

Fig. 5

We used

- entrance vertical slits in 36" : 2" at 26" from the target
- entrance horizontal slits at 36" : 0.835" at 26"

Therefore,

- $d\Omega_e$ = 0.00247 steradian

In fact, the entrance horizontal slits were completely opened and the solid angle in this direction was determined by the vacuum chamber. The equivalent opening at 26" is 0.835" given by:

$$\tan 2d\theta = \frac{W}{R\sqrt{3}} \qquad (2)$$

W = the width of the vacuum chamber at the central radius

R = the mean radius of the magnet.

See article by Judd.[1] Calculation gives $\tan 2\theta d\theta = \frac{W}{R}\sqrt{\frac{n}{n+1}}$. In the present case $n = 1/2$.

- exit horizontal slits 36" : 1.5" at 20" from the magnet face.
- exit vertical slits 36" : 1.5" at 20" from the magnet face.

Case b) Counting of Single Protons

E'_p = 140 Mev (This corresponds to a momentum 530 Mev/c.)

- entrance vertical slits in 72" : 3" or 4" at 28.75" from the target

[1] Judd, Rev. Sci. Instr. 21, 213 (1950).

- entrance horizontal slits in 72" maximum possible : 1.207" at 30.875" obtained by the same way (formula 2).
- exit vertical slits in 72" : completely open, more than 12", the crystals on the multichannel itself determine the used dispersion.
- horizontal exit slits in 72" : 2".

It is usual, when only one counter is used in the 72" spectrometer, to put the vertical exit slits at 54" from the magnet face, because this place corresponds approximately to the focus. When we work with the multichannel, we have to put the plane of all crystals in the focal plane and therefore put the focus between the 5th and 6th channel—in other words place the 5th and 6th channel at 54" from the magnet face.

By counting single protons (with one counter), the curve written "protons" in Figure 6b, shows that there is already an anomalous situation in horizontal slits. Normally we would expect that, in the same way as with vertical slits, the counting rate of single protons might increase proportionately to the slits opening up to the maximum opening 1.2" and after that, stay constant. Apparently this is not the case.

The only reason we could think of, would be that this effect is due to scattering of protons on the horizontal slits and on the walls of the magnet vacuum chamber (5" wide) in such a way that the scattered protons would be counted. A check could be done by using one or two baffles at the entrance and at the middle position of the magnets.

This effect is not seen with vertical slits because the walls in that direction are very far (vacuum chamber 30" high).

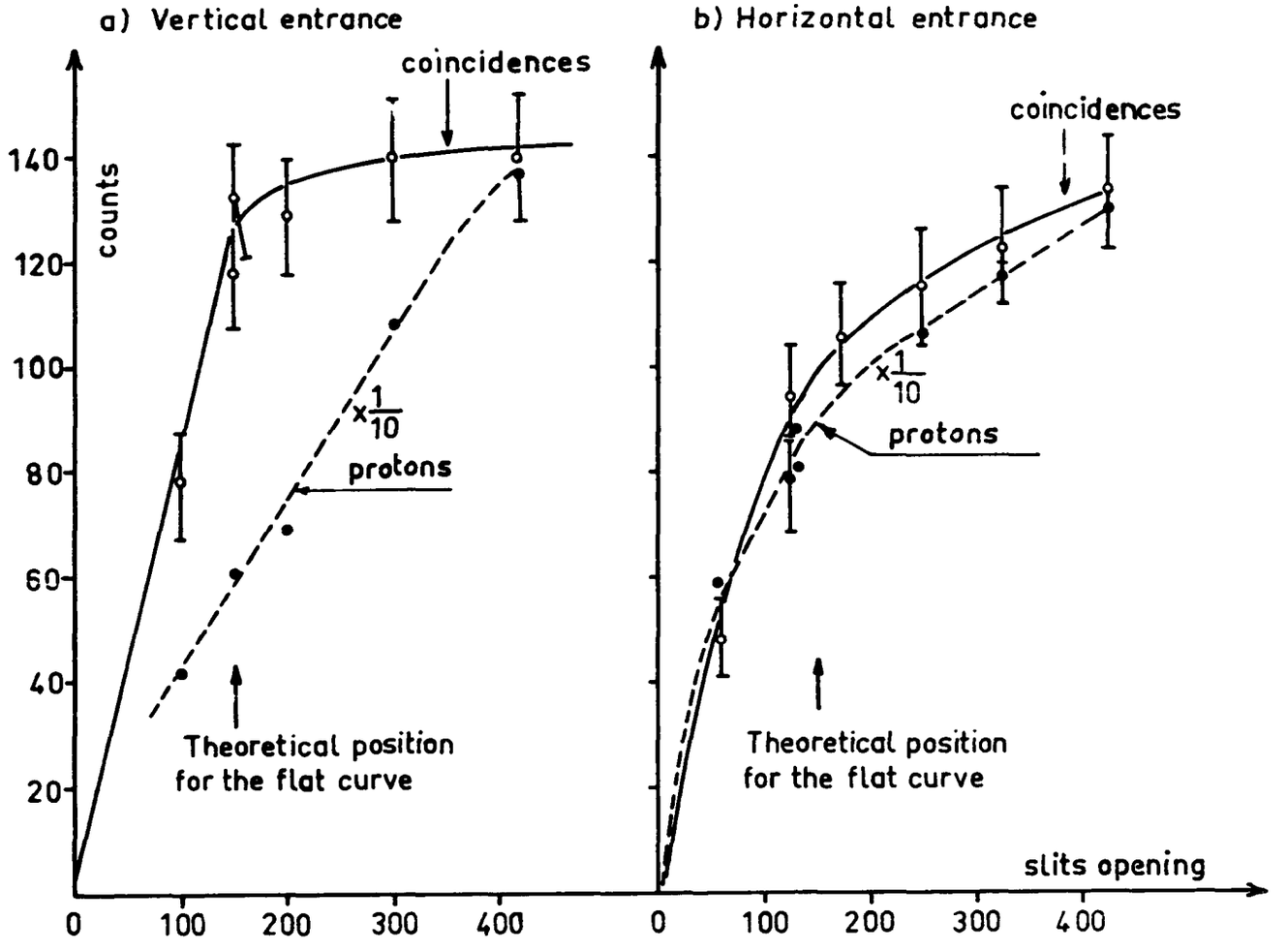
a) Vertical entrance
b) Horizontal entrance
coincidences
counts
140
120
100
80
60
40
20
x 1/10
protons
Theoretical position
for the flat curve
0
100
200
300
400
slits opening

Fig. 6

This effect could be due also to the magnet aberrations. But the "optics" measurements done with an electron beam did not show such an effect.

Case c) Counting of e-p Coincidences

In the cases a) and b), the solid angles $d\Omega_e$ and $d\Omega_p$ are independent. In the detection of the coincidences e-p, the solid angles are correlated by kinematics. We always have the possibility to choose $d\Omega_e$ and open the entrance slits in the 72" in such a way that they define a solid angle bigger than the corresponding $d\Omega_p$ (or inversely, choose $d\Omega_p$ and open the slits in the 36").

If we want to measure an <u>absolute</u> cross section with a d^2 target, we have to be sure at first that we get an absolute cross section by coincidence with a H^2 target. For this reason, we wanted to check if $d\Omega_e$ and $d\Omega_p$ were related in the calculated kinematical way. We did it with only one counter for protons and therefore were not able to have the whole hydrogen peak in the counter at one setting of the current in the 72". We have kept fixed the slits opening for 36" spectrometer and measured with the 72" current setting corresponding to the maximum of the peak. With these conditions, we have counted the coincidences versus the opening of either vertical or horizontal slits. The results are shown in Figure 6.

We expect that the coincidence number increases with the slits opening until $d\Omega_p$ corresponds to the $d\Omega_e$ for electrons and will stay constant when $d\Omega_p$ (or better $d\theta$ and $d\varphi$ defining $d\Omega_p$ in vertical and horizontal directions) becomes bigger than the $d\Omega_{po}$

corresponding to $d\Omega_e$.

The experiment shows that it is true for the vertical slits (Figure 6a) but not for the horizontal slits (Figure 6b).

For the vertical slits, it is only a question of geometry. The opening maximum $d\theta_e$ on the 72" is determined by the planes going through the beam axis and passing by the upper and lower points in the 36" slits opening. With 2" vertical entrance slit opening as indicated above, it must correspond to 1.6" vertical entrance for 72". Figure 6a shows that the coincidence curve is flat beyond this opening. Let us note also that in the vertical direction, the target thickness is the diameter of the beam itself, that is about 1/4".

In the horizontal plane, the kinematics of the reaction is responsible for the slits opening in the 72". A horizontal opening of 0.54" in the 72" should correspond to the 0.835" horizontal opening in the 36". The Figure 6b shows that in fact the number of coincidences increases slowly up to the maximum opening of 1.2".

B. Interpretation

This discrepancy cannot be explained by the multiple scattering of proton against the horizontal slits, because this phenomenon would be also seen with the vertical slits.

It can happen partly because we do not count the whole peak but only its maximum. In fact, when one opens the horizontal slits, more protons with different energies (given by kinematics) enter into the magnet and therefore the resolution of the peak may increase. Under

these conditions, the area under the peak can increase proportionately to the opening of the slits without a proportional change in the height of the peak. This effect can contribute to a change of a few percent, but cannot be the only reason.

We think that the main reason is a thickness target effect. We saw previously that the target was about 1" thick. The calculations above for the horizontal opening in the 72" were done for a thin target centered in O (Figure 7). But if the collision takes place in the point A or B, the minimum and maximum angles for electron detection are λ and μ, to which corresponds by kinematics φ_λ and φ_μ for the recoiling protons.

In our case,

λ = 76° 07 minutes — to which correspond — φ_λ = 39° 49 minutes

μ = 73° 56 minutes — φ_μ = 40° 55 minutes

At the slit, this means slit opening of 1.077". We have further to add to this quantity the slit opening corresponding to the length A B where the reaction can take place.

1" (thickness of the target) × sin (40° 23 minutes) = 0.670"

Therefore, to get an absolute cross-section for H^2, we need a horizontal slit opening of 1.747" if the horizontal slit opening in the 36" is 0.835".

Because the maximum horizontal entrance slits opening in the 72" is 1.2", it is not possible to count all coincidences from hydrogen with one position of the magnet for this target thickness. Therefore if we count coincidences from H^2 with one angular position of the 72" spectro-

Fig. 7

meter, it is impossible to do relative measurements for D^2. If we wish to do so, we have to measure coincidences for H^2 with at least two positions; furthermore we see that we cannot consider doing absolute measurements with this target.

With the new target we ordered ($\frac{5}{16}$" thick), the calculation by taking into account the thickness effect gives a maximum horizontal opening of about 0.900". It will be, therefore, possible to check if the curve of Figure 6b becomes flat beyond 0.900" and then do absolute measurements.

When the new target will be finished, I think it is the first thing to be checked; with the multichannel detector for proton, we will not have the trouble for resolution indicated above.*

*In January, 1962, Donald Aitken checked the new flat target with the multichannel ladder as proton detector. He found that the curve of Figure 6b (coincidence number versus horizontal slit opening) becomes flat beyond an opening of 0.900". Therefore, it seems to be proven that the previous discrepancy came from the target thickness effect.

CHAPTER III

EXPERIMENTAL PROCEDURE

Everything must be tested with a H^2 liquid target. A CH^2 solid target gives so much background from carbon in the proton detection that the proton spectrum is more difficult to find and has many accidental coincidences. Furthermore, the strong angular correlation between the electron and the proton makes it easy to find the coincidences.

(A). Set the two magnets at exactly the right angles. In our case it was

$$\theta_e\ (36") = 75°$$

$$\theta_p\ (72") = 40°\ 23 \text{ minutes}$$

(B). Set the magnet current (or field) on the 36" with the polarity (reverse) for electrons and look at the pulse height spectrum on the multichannel analyser (Figure 3). With the inhibition system, set the discrimination level in the valley of the spectrum.

(C). Take the single electron peak by moving the field by steps smaller than $\Delta E'_e$ given by the exit vertical slits, and the dispersion of the magnet. This peak will serve to evaluate the cross section by counting single electrons. Therefore, it is important to measure the background with an empty target.

Example: at $E_e = 500$ Mev $\theta_e = 75°$, $E'_e = 359$ Mev/c.

The theoretical dispersion of the 36" is 1.337" for 1%.

The correction for dispersion of electrons of about 350

Mev with slits at 20" from the magnet face is negligible (0.99). In this case

$$\Delta E'_e = 359 \times \frac{1.5}{1.337} \times 0.99 = 3.98 \text{ Mev}$$

(D). With the 72" on the polarity (forward) for protons, set the field to get the peak going through the magnet. Adjust the discrimination levels of the 10 scalers, counting the single dynode pulses of the multichannel ladder. This can be done by doing a smooth curve with the H^2 target, or better, by making a flat curve with the D^2 target on the top of the inelastic peak. If the efficiency of all the channels is very different, it may be impossible to get a flat curve with a D^2 target. One can, in this case, give a coefficient of efficiency to each channel and correct later the data from these coefficients. It is good also to check that one gets the right pulse height spectrum out of the counter (for proton, one finds a sharp peak, see Figure 8) on the multichannel analyser. (Do not forget to put the multichannel amplifier on position +.)

When the discrimination levels are adjusted, take a peak with H^2 target and the background from the stainless steel frame with an empty target. This peak will serve also to evaluate the cross section from the counting of single protons.

Usually one setting of the current in the 72" magnet is enough to get the complete peak of H^2. Indeed, the multichannel covers about 3% of the spectrum and the width at one half of the maximum of a H^2 peak is usually less than 2%. It is useful to use more than one setting and change the current in such a way that one has an overlapping of a

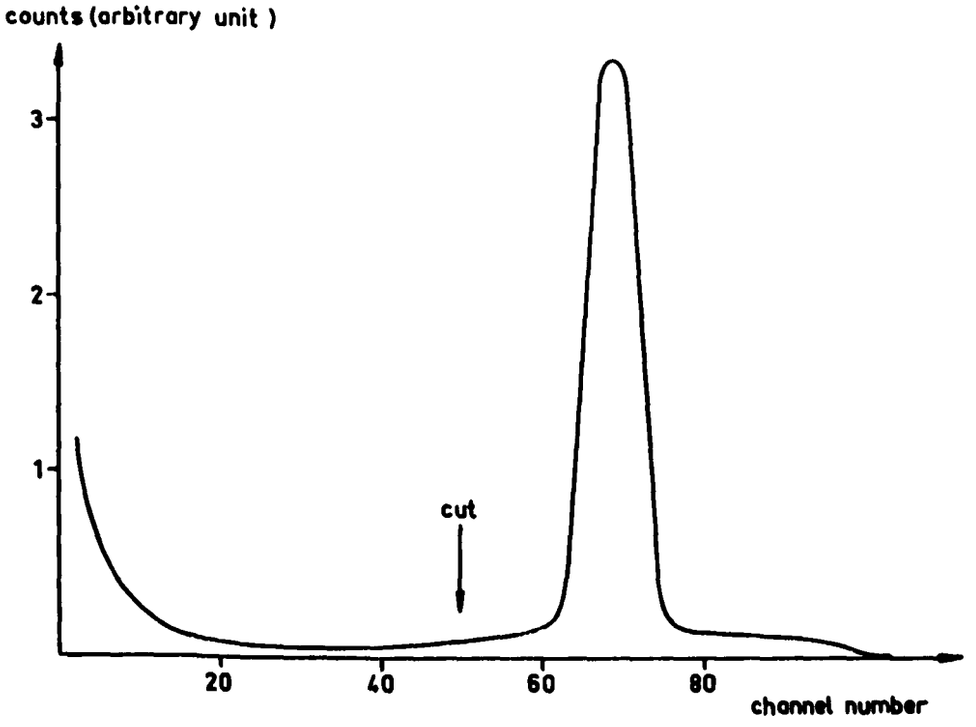

Fig. 8

few channels.

Example: If E_e = 500 Mev

θ_e = 75°

θ_p = 40° 23 minutes P'_p = 535 Mev/c

The theoretical dispersion of the 72" is 2.88" for 1%. The correction for dispersion for 500 Mev/c at 54" from the magnet face is 1.03. Therefore one inch (size of a crystal in the multichannel ladder) corresponds to:

$$\frac{1}{2.88} \times 1.03 \times 5.35 = 1.91 \text{ Mev/c}$$

The separation between the center of two channels is 1.03". Then to move the spectrum of one channel, one has to change the current so that the field is changed by 1.91 × 1.03 = 1.97 Mev/c. To move the spectrum of two channels, we change the field of 3.94 Mev/c; of ten channels, we change the field of 19.7 Mev/c, etc. It is not difficult to do this with the help of the slope curve of the 72" but easier with the rotating coil system.

(E). One can now try to get the coincidences. To do this set the approximate delay between the electron counter and the proton multichannel by taking into account the time of flight of protons and electrons through the magnets, the lengths of cables in different channels and the time delays through the circuits and the different photomultipliers. Do not forget the cable between the splitting circuit for electron pulses and the inputs in the coincidence circuits.

Example: In the case mentioned before, the time of flight of the protons through the 72" magnet is about

55.8×10^{-9} sec. The electron time of flight through the 36" is 13.7×10^{-9} sec. We have about four nanoseconds delay in the cable between the splitting circuit and the coincidences circuits, and eight nanoseconds difference between the time of flight of electrons in the photomultipliers. (RCA 7046 for electron counter and RCA 6810A for proton counters.) Then we have to put an approximate delay of 30 nanoseconds, which means 25 feet of cable RG 63/U.

(F). Set the coincidence bias and the discrimination level on the scalers in order not to count any single pulse. This check can be done by turning off the voltage on either the electron photomultiplier or proton photomultipliers. (Do both checks.)

(G). Check the clipping line length in the coincidence circuits. The protons going through the 72" spectrometer can take different paths and still be detected on the same crystal. The good focusing region for 530 Mev/c momentum is at least 8" out of the central radius of the magnet on each side Therefore some protons follow a curve (that we assume to be approximately a circle) of radius

$$\text{minimum} \quad 72" - 8" = 64"$$

$$\text{maximum} \quad 72" + 8" = 80"$$

For protons of that energy $\beta = \frac{v}{c} = 0.492$. The difference of time of flight at the output is 8.4×10^{-9} sec. The length of the clipping line must be bigger than the length corresponding to this time.

(H). If all conditions indicated above are respected, one finds a narrow coincidence peak.

(I). Now one must set exactly the delay between electron and proton counters by doing delay curves. In principle, the relative delays between the ten channels of the proton side have been previously set (see Chapter II). It is good to check with real coincidences whether the delays are right or not. We mentioned above (section E) that usually the electron pulses come earlier at the input of the coincidence circuit. Therefore, we can insert the box with variable delays in the electron channel before the splitting circuit. By varying the delay in this box, one has one delay curve with each proton channel of the ladder in at the same time. One can check the relative delays in the proton side and set the right delay between the electron and protons channels.

(J). We have two ways to measure a coincidence cross section with a D^2 target.

1). count the coincidences with D^2 alone and calculate directly the <u>absolute</u> cross section from the coincidences numbers,

2). count in the same conditions the coincidences with D^2 and H^2 and, assuming known the cross section for H^2, calculate the cross section for D^2 from the ratio

$$\frac{\text{coincidences number with } D^2}{\text{coincidences number with } H^2}$$

This is a <u>relative</u> measurement.

As we said before (at the end of Chapter II), it is not possible to measure a relative cross section for D^2 with the ine inch thick target and one setting for the angle of the 72" spectrometer, because we cannot have all coincidences for H^2.

Therefore it is very important in order to get any data to use two or three angle settings until we have the new liquid target.

When we have it, the first thing to do will be to solve the slits problem and check if the interpretation of the discrepancy between calculation and experiment if right. If it is so, we can measure absolute cross sections as well as relative for the diffusion by D^2 target. But in any case, it is safer and better to do both. The results must fit and the measurement of the cross section with H^2 is a check that all instruments and apparatus involved work properly.

(K). We have to note also the following (already mentioned):

1) For a measurement with a H^2 target, the entrance solid angle of the 72" magnet $d\Omega_p$ is not involved in the calculation if it is bigger than $d\Omega_{po}$ corresponding to $d\Omega_o$ (Chapter II).
2) For a measurement with a D^2 target, $d\Omega_p$ is independent of $d\Omega_o$ and is a direct component used in the calculation.

(L). Before taking any data, it is necessary to evaluate the efficiency in coincidences of all electronic equipment. It cannot be done with a D^2 target as we do for a single channel, because the counting rate is very low and in coincidences the maximum of the inelastic peak

is no longer a flat curve. We have done it with a H^2 target. In one setting of the current, we have the H^2 peak in coincidence (Figure 5b). We changed the current in such a way that each crystal of the ladder counts the whole peak (Figure 9). By comparing the area under the ten peaks, we can give an efficiency factor to each channel. In fact, all efficiencies were found near 100% and the curves are not affected by this correction factor.

(M). Finally to take data, we count the coincidences with D^2 or H^2 for a certain integrated beam in the Faraday cup. We sometimes changed the 72" current in such a way that the protons counted in one channel during a measurement would be counted in another channel in the second measurement. With this method, we have an average of cancellation of different possible corrections and permanent check for all ten circuits and channels. An example is given on Table I.

(N). The accidental coincidences are not a negligible percentage of the real coincidences. It is important to count them quite often. We thought of differing solutions in order to avoid them, but apparently we would decrease the real counting rate in such a way that we would not gain anything. The main trouble is that we cannot use a better time resolution because of the different times of flight of protons through the 72" magnet.

(O). To get the coincidences cross section from H^2, we have to count all coincidences e-p which correspond to the single electron peak (Figure 4). To plot this single peak, we used many steps smaller

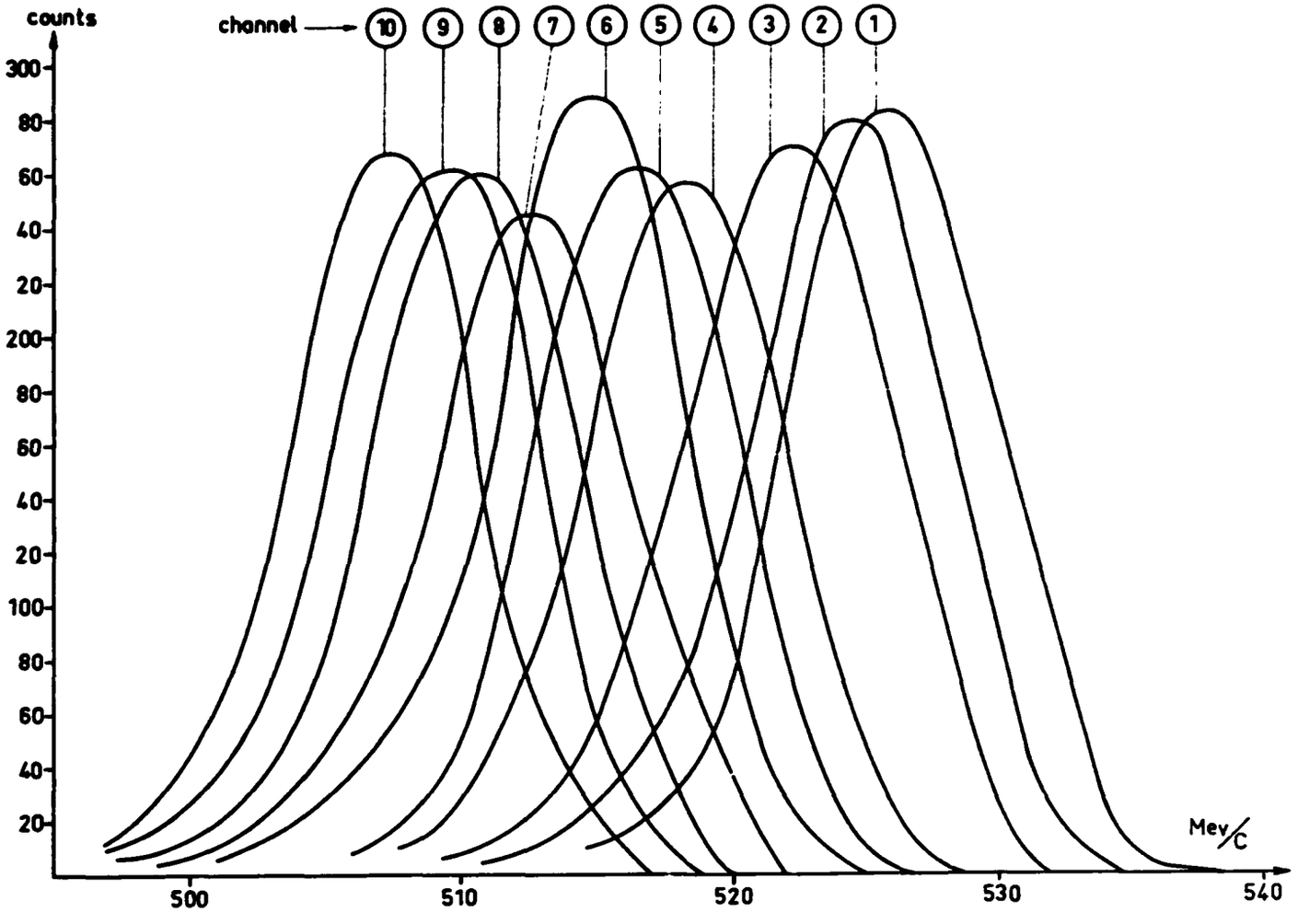
counts
channel
10
9
8
7
6
5
4
3
2
1
300
80
60
40
20
200
80
60
40
20
100
80
60
40
20
500
510
520
530
540
Mev/c

Fig. 9

D² TARGET REAL COINCIDENCE

Ep of each channel	501	503	505	507	509	511	513	515	517	519	521	523	525	527	529	531	533	535	537	539	541	543
Field Setting																						
520						3.7	10	2.8	16	12.4	19	21.6	24	[illegible]	21.5							
526									11.1	9	19.7	25	27.9	38	21.5	21	13	16.1				
500	3	4.3	4	5	2.1																	
540																19.4	14	6.6	15	3.1	4	1.1
526									17.6	18	32.9	32	43.4	41	25.9	23	28	9.7				
540																24.1	20	14.1	17	13.4	11	2.1
508	14	8.9	16	17.6	19	10.8	20	18	17.2													
520						10.2	14	16	27	29.9	25	23.7	29	28	33.3							
528								12	24	24.1	33	37.2	32	33.4	37	29	22.5					
526									25	32	28.2	32	28.2	32	16.2	18	9	7.5				
Total	17	12.8	20	22.6	21.1	24.7	44	48.8	137.9	115.4	157.9	171.5	194.5	195.4	155.4	134.5	106.5	54	32	16.5	15	3.2
±	4	3	4.5	5	4.5	5	7	7	12	11	12	13	14	14	12	12	10	7	6	4	4	2
Total for 1800/ucb	51	38.4	60	67.8	63.3	49.4	88	73.2	113.2	115.4	157.9	171.5	194.5	195.4	155.4	134.5	106.5	64.8	96	49.5	45	10
±	12	9	13	15	13	10	14	11	11	11	12	13	14	14	12	12	10	9	10	10	12	12

A C C I D E N T A L

526									7.4	1	9	9	9.3	8	8.6	9	2	2.1				
508	1.1	10.3	19	19.6	9	8.6	14	11	5.4													
526									5.5	9	4.7	14	13.4	10	5.4	8	9	5.4				
526									4.3	13	7.5	27	10.3	12	4.3	15	1	3.2				
Total	1.1	10.3	19	19.6	9	8.6	14	11	26.6	23	13.1	50	33	30	18.3	32	12	10.7				
Total for 1800/ucb	6.6	61.8	114	117.6	54	51.6	84	66	40	46	26.2	100	66	60	36.6	64	24	22.1				
±	7	20	30	30	18	18	24	20	6	10	7	14	12	12	10	12	18	10				

TABLE I.

than $\Delta E'_e$ determined by the exit energy slits of the 36" spectrometer. With coincidence, this method would require a long time. It is easier and as precise (we verified it several times) to use only a few steps in such a way that the next one follows the previous one without overlapping. We can calculate with the slope curve or with the rotating coil system how much we have to move the current to have the new setting (see Figure 4).

For example, in our case, we saw (Chapter III section C) that we get almost the complete peak with only three settings: 358 Mev, 354, and 350 Mev.

Therefore to measure the coincidences with H^2, we have to add the coincidences from the three settings.

For the cross section of the diffusion by D^2, one setting only of the 36" current is necessary because $\Delta E'_e$ is already involved in the calculation.

The coincidence spectra with D^2 and H^2 targets are shown in Figure 10. The H^2 spectrum is to show the position of the peak relative to the D^2 peak, not for evaluation.

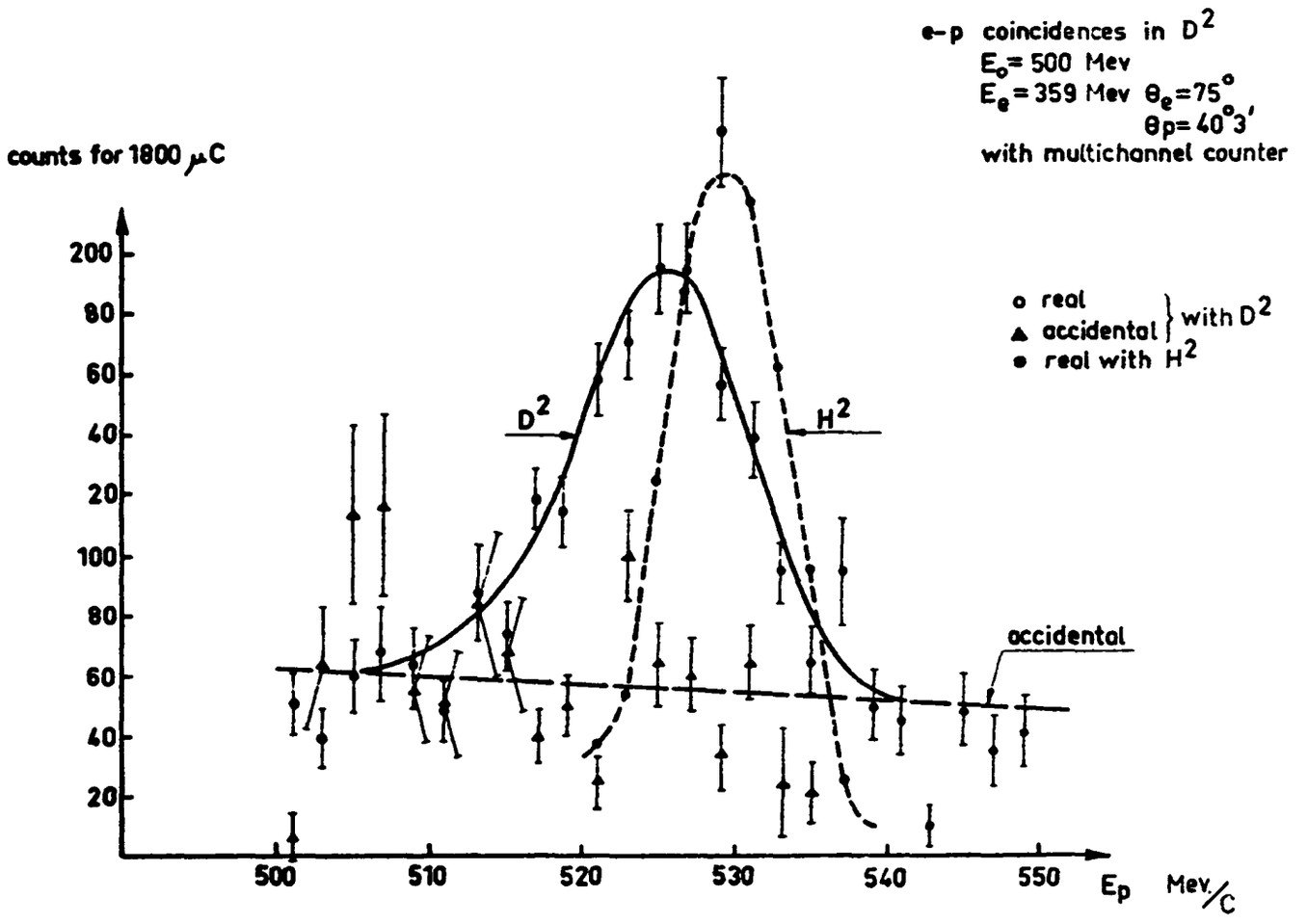
e–p coincidences in D^2
E_o = 500 Mev
E_e = 359 Mev $\theta_e = 75°$
$\theta p = 40°3'$
with multichannel counter
counts for 1800 μC
o real
▲ accidental } with D^2
● real with H^2
D^2
H^2
accidental
200
80
60
40
20
100
80
60
40
20
500
510
520
530
540
550
Ep Mev/c

Fig. 10

CHAPTER IV

RESULTS

Although it was not possible to get even a relative cross section for D^2 (we used only one angle setting for the 72"), we will show the results obtained. We think they are exact within 20 or 30%, because the lost counts with H^2 target were not more than these percentages. In any case, the same calculation must be followed to find the cross section from the new data.

(A). The cross section with D^2 target is found from:

$$\frac{d^3\sigma}{d\Omega_p\, d\Omega_e\, dE'_e} = \left(\frac{d\sigma}{d\Omega}\right)_{\text{proton}} \frac{N_D\, R_D}{C_D}\, \frac{C_p}{N_p\, R_p}\, \frac{1}{d\Omega_p\, dE'_e}$$

where,

$\left(\frac{d\sigma}{d\Omega}\right)_{\text{proton}}$ = is the elastic scattering cross section by a H^2 target

$N_D\, N_p$ = is the coincidences numbers with a D^2 and H^2 target

$R_D\, R_p$ = is the radiative corrections to be applied to the numbers $N_D\, N_p$ to get the real number of counts to be used.

$C_D\, C_p$ = is the charges on the Faraday cup accumulated during the time to count N_D and N_p

$d\Omega_p$ = is the entrance solid angle of the proton magnet

dE'_e = is the energy spread of the electron counter

defined by the exit slits in the 36" spectrometer.

(B). Example: With the experimental conditions already indicated we have measured the cross section with H^2 and D^2 target.

E_o = 500 Mev

E_e = 359 Mev θ_e = 75°

E_p = 535 Mev/c θ_p = 40° 23 minutes

N_p = 1497 ± 41 C_p = 60 microcoulombs R_p = 1.20

(see Chapter IV, section C for radiative correction)

N_D = 630 ± 53 C_p = 1200 μc R_D = 1.136

(see Chapter IV, section C)

$d\Omega_p$ = 3.38/1000 steradian

dE'_e = 3.98 Mev (see Chapter III, section C)

To take into account the thickness effect (Chapter II and curve 6) we assume that N_p is too low by a factor about 20%.

We therefore will take $N_p = 1497 \times 1.2 = 1796$

$$\left(\frac{d\sigma}{d\Omega}\right)_{\text{proton}} = 3.6 \times 10^{-32} \text{ cm}^2/\text{ster.}$$ (Chapter IV, section D)

The calculation gives finally:

$$\frac{d^3\sigma}{d\Omega_p\, d\Omega_e\, dE'_e} = 4.7 \pm 0.5 \times 10^{-32} \text{ cm}^2/\text{ster}^2 \text{ Mev.}$$

The measurement done in another run gave by the same way:

$$\frac{d^3\sigma}{d\Omega_p\, d\Omega_e\, dE'_e} = 3.70 \pm 0.4 \times 10^{-32} \text{ cm}^2/\text{ster}^2 \text{ Mev.}$$

The two results are very different one from the other. This effect is due to the fact that the horizontal entrance slits were not the same

for the two runs.

We will take as a result:

$$4.2 \pm 0.6 \text{ cm}^2/\text{ster}^2 \text{ Mev}$$

(C). Radiative correction. We will discuss here the radiative correction to be applied in the e-p coincidence experiment with a hydrogen target. We will see, after that, what must be done about the deuterium target measurements.

Let us call E_1 the part counted in the single electron peak (Figure 11a) and E_2 the part not counted. When one detects only electrons, the radiative correction is roughly $R_{pe} = \frac{E_1 + E_2}{E_1}$. By the same way (Figure 11b), by detecting only protons the radiative correction is $R_{pp} = \frac{P_1 + P_2}{P_1}$. The problem arises: What is the radiative correction to be applied when one detects e-p coincidences?

1) We know that the spectrum part E_2 is due to several causes: a) the electron energy loss on the path AO (Figure 11c)(bremsstrahlung thickness effect), b) the electron energy loss on the path OC (bremsstrahlung thickness effect), c) the electron energy loss on the point O (Schwinger correction).

2) By the same way, P_2 is due to: a) electron energy loss on the path AO bremsstrahlung, b) proton energy loss on the path OB, c) proton energy loss on the point O. (Energy losses of b) and c) are not known. On the path OB we can assume that it is negligible.) On the point O, Tsai is calculating the correction,

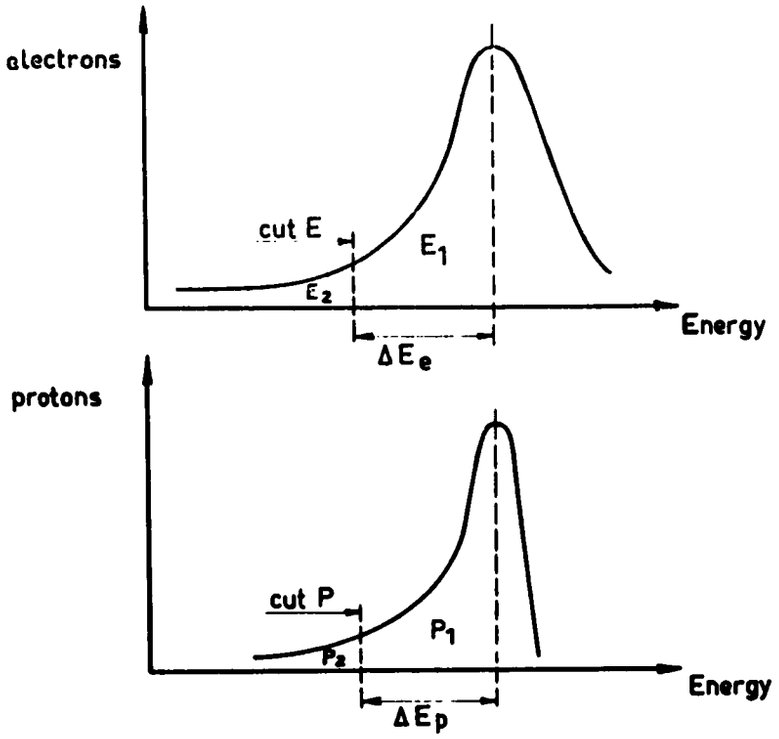
electrons
cut E
E_1
E_2
Energy
ΔE_e
a.)
protons
cut P
P_1
P_2
Energy
ΔE_p
b.)

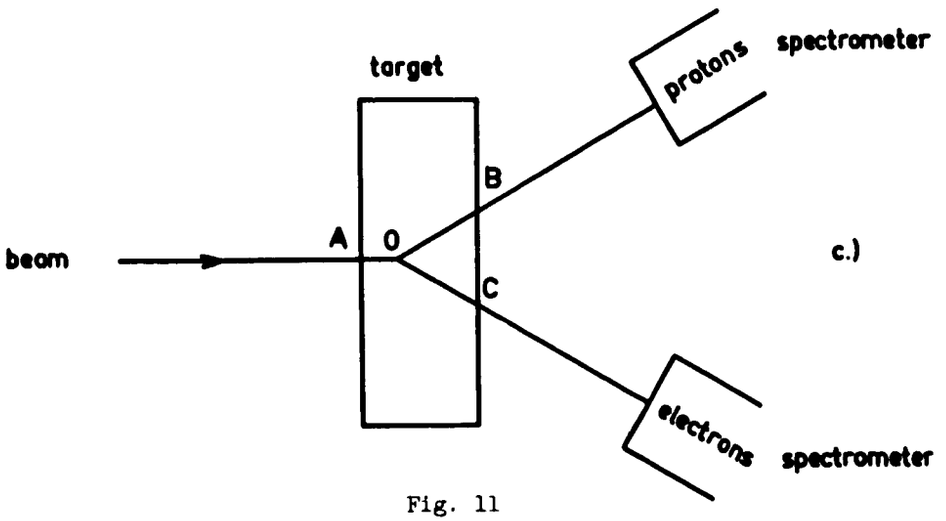
target
protons
spectrometer
B
A
0
beam
C
electrons
spectrometer
c.)

Fig. 11

it may be only a few percent and we neglect it.*

We therefore see that the radiative correction from the detection of only single protons is lower than that from electron detection.

3) When we measure e-p coincidences, we have to see from which part of each spectrum a coincidence may take place. We give only a qualitative understanding of the problem. It should be completed by calculations.

   a) Without any loss anywhere one can count a coincidence from E_1 and P_1.

   b) If an energy loss takes place in the path AO, the incident energy is lower in O and proton and electron energies are lower. The radiative correction to be applied depend mainly on where the cutting positions P and E in the electron and protons peaks are. (Figures 11a and 11b).

   c) If ΔE_p is relatively wide, a proton in P_1 may be detected with an electron in E_1 or E_2.

   d) If ΔE_p is narrower, we may also have a proton detected in P_2 and an electron in E_1 (or E_2). If the energy loss is big in AO, protons will be detected in P_2, but electrons probably have energy low enough to be counted in E_2 and this coincidence is not counted.

*Allan Krass calculated the correction. It has to be taken into account.

e) If the bremsstrahlung comes on OC, the electron may be in the E_2 part. But, because bremsstrahlung radiation is emitted after the collision, the kinematics is not changed for the proton and the proton is still counted in P_1.

f) The Schwinger radiation is mainly emitted in the same direction as the scattered electron during the collision. Therefore kinematics is not changed for the proton and the proton is still counted in P_1.

Finally, all protons counted in P_1 are in coincidence with the E_1 and E_2 part of the single electron peak (section C, number 3, items c, e, f, of this chapter). In this case, we have to apply the radiative correction for single electron spectrum only.

We have to apply another correction for the case in item d, but it would be small if ΔE_p corresponds to more than 1%.

If in the Tsai calculation the Schwinger correction in the proton detection appears not to be negligible, it would have to be included.

For Hydrogen the radiative correction is therefore R_{pe}.

For deuterium, we can follow the same method and apply as radiative correction the one for the peak height of the inelastic scattering because we detected electrons on the peak maximum and not the whole inelastic peak.

We apply the Sobbotka formula, because it gives within a few percent the same results as the Tsai formula and is simpler.

(D). The elastic scattering cross section $\frac{d\sigma}{d\Omega}$ with a hydrogen target is the usual Rosenbluth formula with the form factors F_{1p} and F_{2p}. In that example,

$$q^2 = 6.8\ f^{-2} \quad (f = 10^{-13}\ \text{cm})$$

The values taken from the latest work on proton are

$$F_{1p} = 0.56$$
$$F_{2p} = 0.45,$$

which give the indicated cross section

$$\frac{d\sigma}{d\Omega} = 3.6 \times 10^{-32}\ \text{cm}^2/\text{ster}.$$

If we want to compare it with the exponential model which gives still a good fit for the cross section at this q value, we find

$$\frac{d\sigma}{d\Omega} = 3.77 \times 10^{-32}\ \text{cm}^2/\text{ster}.$$

if we assume a rms radius $a = 0.8\ f$ and use therefore,

$$F_{1p} = F_{2p} = 0.537.$$

CHAPTER V

INTERPRETATION OF THE RESULTS

A. Introduction

In this experiment, we want to check to see if the proton form factors are the same in a bound as in the free state. A difference could be interpreted as a meson exchange effect between the proton and the neutron during the electron deuteron collision.

This check can be done by measuring the differential cross section $\frac{d^3\sigma}{d\Omega_p\, d\Omega_e\, dE'_e}$ in the direction of the proton detection corresponding to the momentum transfer q for a free proton (see below).

L. Durand[2] and J. Scofield[3] studied the angular distribution of the outgoing nucleons from an inelastic electron deuteron scattering.

Durand gives the differential cross section in the center of mass system of outgoing nucleons. We use his formula and a center of mass to lab system transformation formula due to Scofield.[3] Besides, the Durand's results fits with the cross section found by Scofield directly in the lab system.

B. Connections Between our Measurement and the Durand's Formula

For the first attempt in this problem, we chose to measure at a place where the calculations were already done by Durand. That is:

---

[2] Durand, Physical Review 115, 1020 (1959)

[3] Scofield, private communication.

incident beam E_o = 500 Mev

scattered electron angle θ_e = 75°

With an hydrogen target, the proton is emitted in an only direction, which is the momentum transfer direction q. In this case

$$\theta_p = 40° 23 \text{ minutes}$$

With a deuterium target, the cone in which the protons are emitted for a given scattered electron energy is wider and no longer a δ function. The q direction is a symmetry axis. With this direction q taken as the origin of angles and in the center of mass system of outgoing nucleons, the cross section is given in the equation 11.1 (simplified case) or equation 1-4 of appendix I (with relativistic correction) of Durand's paper.*

Because the relativistic corrections are still small (for example they are about 2% for the proton energy and the corrections on the cross sections must be of the same order) and this measurement was a first attempt to get a differential cross section, we have used only the simplified case (equation 11.1 D).

We see that the cone is in fact the whole space, but the cross section for an energetic proton is big only in a cone of about 30°. (See Figure 1 D and Figure 2D). For Figure 1 D the curve must be divided by sin θ to get the differential cross section. For Figure 2 D the differential cross section is obtained by squaring the function $f(\theta)$.

---

*We will refer to equations from Durand by using the letter D after the equation number.

In the lab system, the cone is still smaller and we need to go only up to 15° around q to get the whole angular distribution. We give in Figure 12 the proton momentum where the coincidence peak is expected to appear. This plot is done from the relation:

$$\vec{P}_p = 1/2\ \vec{q} + \vec{p} + q(E_e - E'_e + 2M - 2E)\ \frac{p \cos\theta}{2E} \qquad (3)$$

obtained from (appendix I - I-6 D) which gives the lab energy of the neutron in the relativistic case. In the non-relativistic approximation

$$P_p = 1/2\ \vec{q} + \vec{p}$$

gives practically the same curve. By restricting outselves at a forward angle ($\theta_{CM} < 10°$), we see that, in first approximation, we can neglect the contribution of the second and the third term of (11.2 D) and (Figure 1 D). Therefore the Durand's formula becomes:

$$\frac{d^3\sigma}{d\Omega_p\ d\Omega_e\ dE'_e} =$$

$$\sigma_{Mott}\ \frac{Mp}{4\pi^2h^2}\ F^2(\theta)\ F_1^{\,2} + \frac{hg}{2Mc}^{\,2}\ 2(F_1 + K_pF_2)^2\ \tan^2\frac{\theta}{2} + F_2^{\,2}\ K_p^{\,2} \qquad (4)$$

We have included a factor 2π (to get $d\Omega_p$) and the form factors F_1 and F_2. The bracket on the right side of formula (4) is the Rosenbluth factor in the cross section for a free proton. In our case

$$\sigma_{Mott}\ \frac{Mp}{4\pi^2h^2} = \frac{4.71}{2\pi} \times 10^5\ \text{cm}^{-1}\ \text{ster}^{-2}\ \text{Mev}^{-1}$$

With the values taken above for the proton form factors F_1, F_2 the Rosenbluth bracket is 0.529 and the angular distribution at forward angles in the cneter of mass system is:

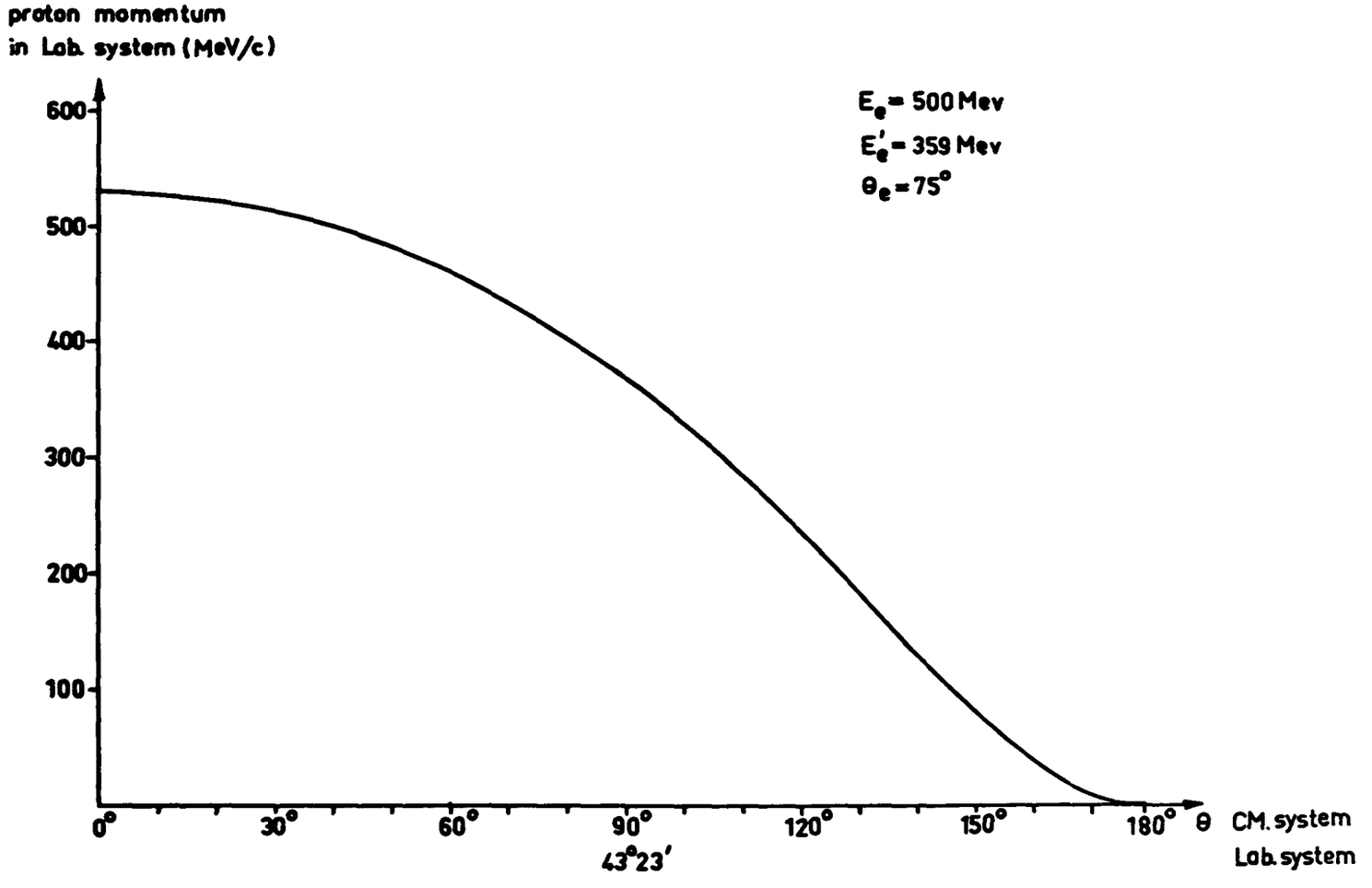
proton momentum
in Lab. system (MeV/c)
600
500
400
300
200
100
E_e = 500 Mev
E'_e = 359 Mev
θ_e = 75°
0°
30°
60°
90°
43°23'
120°
150°
180°
θ
CM. system
Lab. system

Fig 12

$$\frac{d^3\sigma}{d\Omega_p\, d\Omega_e\, dE'_e} = 3.97 \times 10^4 \;\; F^2(\theta) \;\; cm^2 \;\; ster^{-2} \;\; Mev^{-1}$$

Scofield calculated the center of mass to lab system transformation for the cross section. His result is

$$\frac{|P_p|^3 \, d\Omega_{pp}}{(E_n \vec{P}_p - E_p \vec{P}_n) \cdot \vec{P}_p} = \frac{|\vec{P}|}{2E} d\Omega_p \qquad (5)$$

where everything on the left side is evaluated in the lab system and everything on the right side in the center of mass system.

P_p and P are the momentum of the proton.

E_p and E are the total energy of the proton (with the rest mass energy).

E_n is the total energy of the neutron.

In our first experimental case (proton emitted in q direction), we have

$$P_n = 0$$

$$E_n = M$$

Therefore,

$$\frac{P_p}{M}(d\Omega_p)_{lab} = \frac{P}{2E}(d\Omega_p)_{CM}$$

This gives,

$$\frac{d\Omega_{CM}}{d\Omega_{lab}} = 4.86$$

Finally,

$$\frac{d^3\sigma}{d\Omega_p\, d\Omega_e\, dE'_e}_{Lab} = 1.93 \times 10^5 \;\; F^2(\theta) \;\; cm^2 \;\; ster^{-2} \;\; Mev^{-1}$$

To get $F(\theta)$, we can use the formula 11-3 D. For the Hulthen radial wave function:

$$u(r) = N(e^{-\gamma_1 r} - e^{-\gamma_2 r})$$

with

$$N = 2.77 \times 10^{6}$$

$$\gamma_1 = 2.31 \times 10^{12}\ \text{cm}^{-1}$$

$$\gamma_2 = 6.21\ \gamma_1$$

we find

$$F(0) = 4.98 \times 10^{-19}$$

We could have calculated $F(\theta)$ from only 11.3 D. But at this early stage of the calculation, we think that it is as good to use the curve given by Durand in his Figure 2.* In principle this curve is not right because the radial wave function is no longer (8-1-D) but the function of appendix II (II-I D). But in first approximation, it is good because $G^2(\theta)$ is small at forward angle ($\theta \leq 5°$) and negligible compared to $F^2(\theta)$ (see Formula II-4 D).

If we use this curve, we find

$$F(0) = 4.90 \times 10^{-19}$$

which differs from the value indicated above by 1.6%. Furthermore, according to the γ_2 value (that we can change slightly because the wave function is not known so accurately), $F(0)$ can vary more than 1.6% and therefore we are justified to use this curve to calculate $F(\theta)$. From the foregoing considerations we have:

---

*On page 1037 of Durand's paper, two typographic errors exist: a) in Figure 2 correct $f = (\ )F$ to read $F(\theta) = (N/\alpha^2)\cos f(\theta)$, b) at the end of the same column, correct 10^{13} to read $\alpha^{-1} = 4.31 \times 10^{-13}$ cm.

$$\left.\frac{d^3\sigma}{d\Omega_p\, d\Omega_e\, dE'_e}\right|_{\substack{\theta=0 \\ \text{Lab}}} = 4.63 \times 10^{-32}\ \text{cm}^2/\text{ster}^2\ \text{Mev}$$

By the same way, we can find the angular distribution at forward angle. The result is shown in Figure 13.

We checked this curve only at $\theta = 0°$ with the Scofield's theory which gives directly the differential cross section in the lab system. Instead of 4.63×10^{-32} found with the Durand's theory, we get

$$\left.\frac{d^3\sigma}{d\Omega_p\, d\Omega_e\, dE'_e}\right|_{\substack{\theta=0 \\ \text{Lab}}} = 4.85 \times 10^{-32}\ \text{cm}^2/\text{ster}^2\ \text{Mev}.$$

The two results differ only by 4%. We consider that they fit correctly.

C. Comparison of our Result with the Theory

We must be cautious in comparing the experimental result with the theory. The angular distribution is sharply peaked at small angles and therefore the cross section varies very rapidly when we are not at $0°$. For instance, at $3°$ in the lab system out of the q direction, the cross section is about one half of its maximum at $0°$. In the other hand, $d\Omega_p$ is finite and Figure 14 shows that the maximum angle may be about $3°$.

We have calculated an average of the cross section in the experimental $d\Omega_p$ by cutting the slits opening in several sections from number 1 to 6 (Figure 14) and, for each section we used the theoretical cross section for the mean angle. By doing this, we assume that the

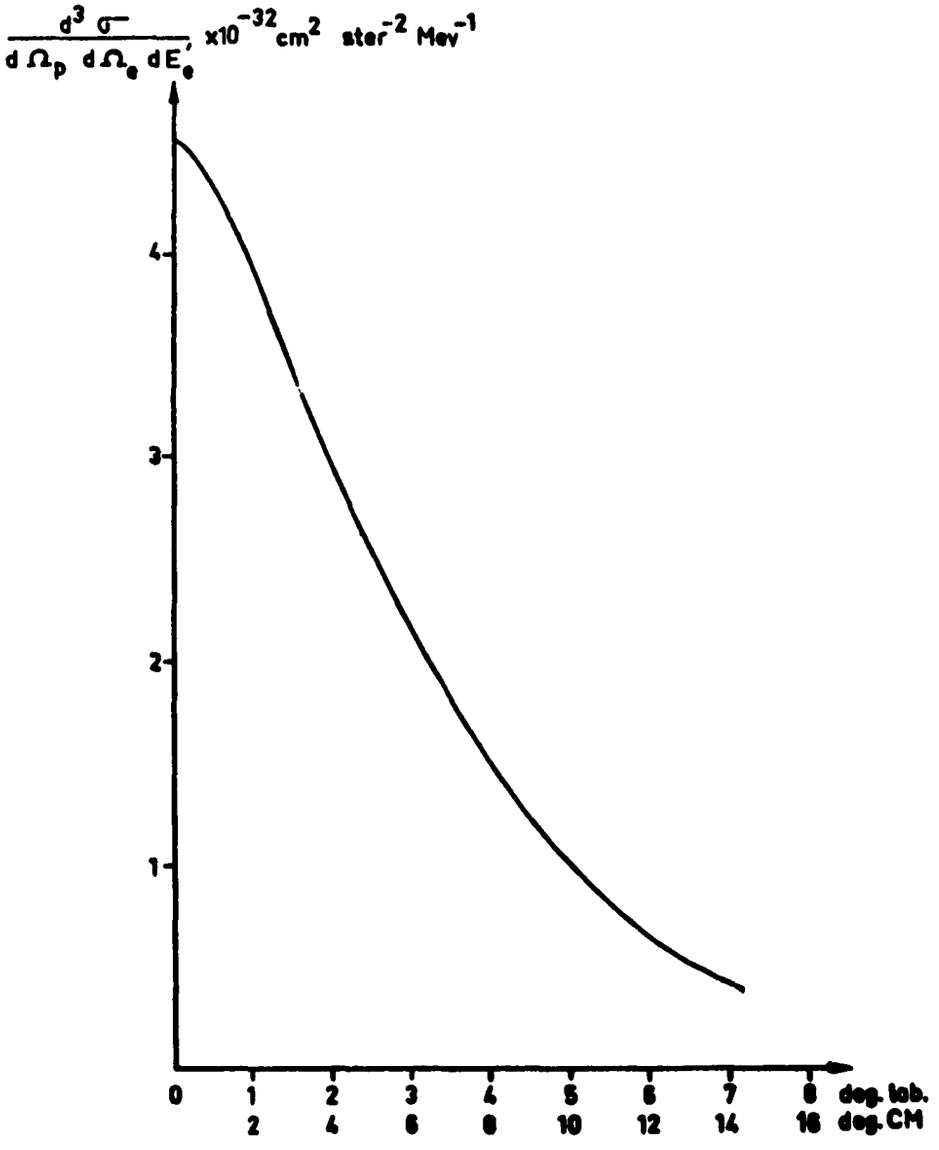
$\frac{d^3\sigma}{d\Omega_p\, d\Omega_e\, dE_e'}$ x10^{-32}cm^2 ster^{-2} Mev^{-1}
4
3
2
1
0
1
2
2
4
3
6
4
8
5
10
6
12
7
14
8
16
deg. lab.
deg. CM

Fig. 13

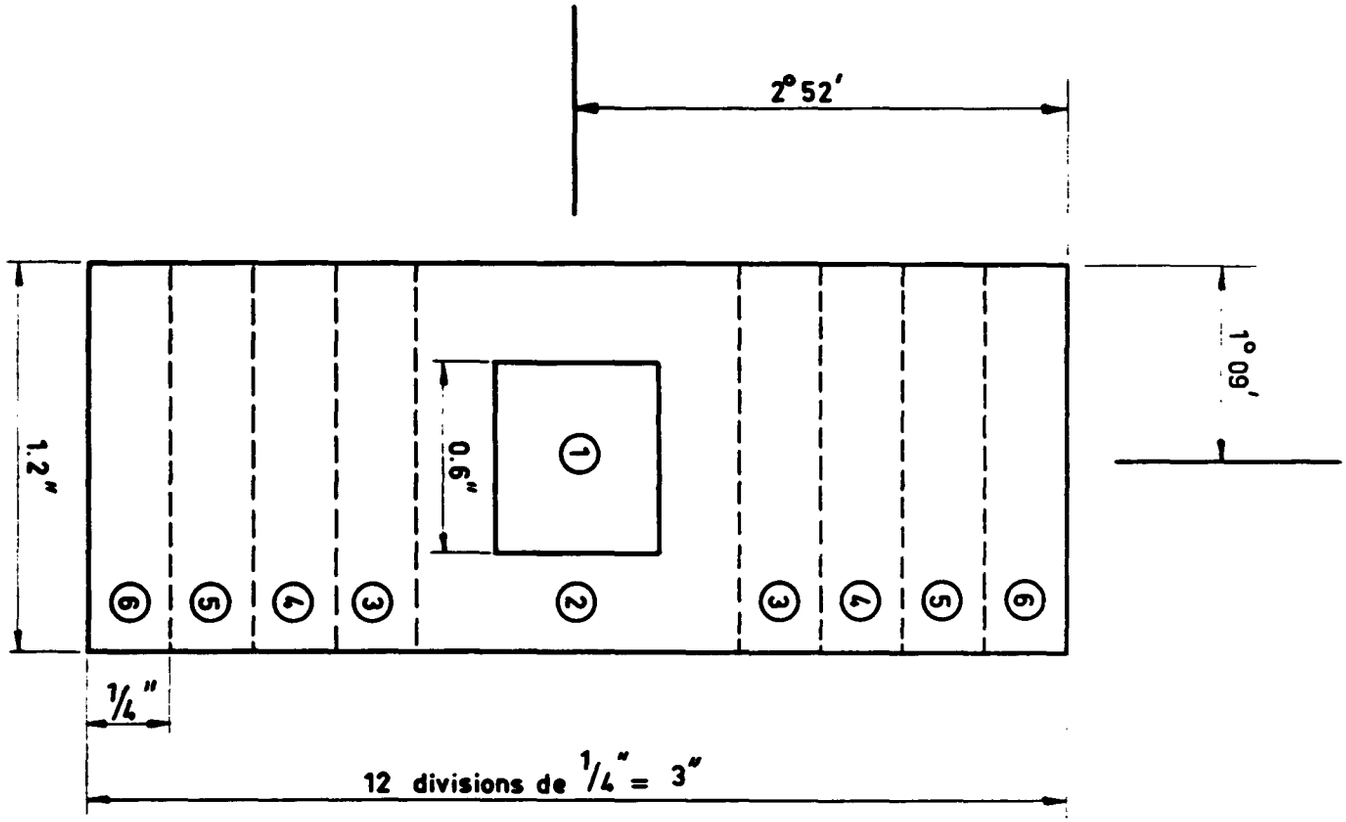

Fig. 14

angular distribution has an axial direction about the q direction. We believe it is so, because we do not see any apparent reason why the symmetry would be broken.

In these conditions, the theoretical average becomes:

$$\left(\frac{d^3\sigma}{d\Omega_p\, d\Omega_e\, dE'_e}\right)_{\substack{\text{average} \\ \theta=0}} = 3.37 \times 10^{-32}\ \text{cm}^2/\text{ster}^2\ \text{Mev}.$$

CHAPTER VI

CONCLUSION

The experimental value $4.2 \pm 0.5 \times 10^{-32}$ cm^2/ster^2 Mev does not seem to fit perfectly with the theoretical values 3.37×10^{-32}. We can explain this discrepancy of the order of 20% by several reasons:

a) The experimental values are not known with a good accuracy and because of the slits problem, cannot in the present stage of the problem, be trusted within 20 or 30%.

b) In the calculations, some approximations have been done in the application of the formula.

c) In the theory itself, the cross section depends on the deuteron wave function and on the final state interaction. It would be useful to perform the calculations with a wave function more realistic such as one with a repulsive core potential.

d) Because of the meson exchange effect, proton form factors in a bound state may be different from those in the free state. But before thinking of this reason, the three other points must be brought out.

e) Although the theory and the experiment do not fit perfectly, we think that we have reached our first goal, which was to find the coincidences and compare the first order with the theory. We found a cross

section which differs only by 20% of the expected value and not by an order of 10 or 100 which would have been possible with all points which are to be considered.

We have shown that this tool may be useful and that the method is possible. Accurate measurements and refinements in the theory may give in the future some good results.

DISTRIBUTION LIST

Contract Nonr-225 (67)

Government

Professor W. K. H. Panofsky
Department of Physics
Stanford University
Stanford, California

Mr. J. R. King
ONR Res. Rep.
Stanford (ERL)

P. B. Fine
Microwave Laboratory
Stanford University
Stanford, California

SLAC Library
Stanford University
Stanford, California

Margaret Rabbinowitz
Physics Department
Stanford University
Stanford, California

Commanding Officer
Office of Naval Research Branch Office
1000 Geary Street
San Francisco 9, California

U. S. Atomic Energy Commission
Patent Branch
Washington 25, D. C.

Office of Technical Services
Department of Commerce
Washington 25, D. C.

Commanding Officer
Office of Naval Research Branch Office
1030 East Green Street
Pasadena 1, California

Commanding Officer
Office of Naval Research Branch Office
John Crerar Library Bldg.
86 East Randolph Street
Chicago 1, Illinois

(6) Director, Naval Research Laboratory
Attn: Technical Information Officer
Washington 25, D. C.

Chief of Research and Development
Department of the Army
Washington 25, D. C.

U. S. Atomic Energy Commission
New York Operations Office
70 Columbus Avenue
New York 23, New York

(5) Armed Services Technical Information Agency
Arlington Hall Station
Arlington 12, Virginia

(2) Chief of Naval Research
Attn: Nuclear Physics Branch, Code 422
Department of the Navy
Washington 25, D. C.

Chief, Physics Branch
U. S. Atomic Energy Commission
Washington 25, D. C.

Exchange and Gift Division
Library of Congress
Washington 25, D. C.

(3) Commander
Air Force Office of Scientific Research
ARDC, Attn: SRPN
Washington 25, D. C.

U. S. Atomic Energy Commission
Technical Information Service Extension
Attn: Document Processing Branch
P. O. Box 62
Oak Ridge, Tennessee

Oak Ridge National Laboratory
Attn: Head, Physics Division
P. O. Box P
Oak Ridge, Tenn.

Ames Laboratory
Iowa State College
P. O. Box 14-A, Station A
Ames, Iowa

Argonne National Laboratory
Attn: Hoylande D. Young
9700 South Cass Avenue
Argonne, Illinois

Chief, Burear of Ships
Attn: Code 300
Department of the Navy
Washington 25, D. C.

Library and Record Center
Monsanto Research Corporation
Mound Laboratory
P. O. Box 32
Miamisburg, Ohio

Chief, Burear of Naval Weapons
Attn: DLI-3
Department of the Navy
Washington 25, D. C.

Librarian
U. S. Naval Postgraduate School
Monterey, California

Chief, Bureau of Naval Weapons
Attn: RRSY-3
Department of the Navy
Washington 25, D. C.

Chief, Bureau of Naval Weapons
Attn: RR-12
Department of the Navy
Washington 25, D. C.

Sandia Corporation
Classified Document Division
Albuquerque, New Mexico

Superintendent, Nucleonics Division
Naval Research Laboratory
Anacostia, Washington, D. C.

Chief, Bureau of Ships
Attn: Code 1500
Department of the Navy
Washington 25, D. C.

National Bureau of Standards of
Library
Room 301, Northwest Bldg.
Washington 25, D. C.

Knolls Atomic Power Laboratory
Attn: Document Librarian
P. O. Box 1072
Schenectady, New York

Los Alamos Scientific Laboratory
Attn: Report Library
P. O. Box 1663
Los Alamos, New Mexico

Brookhaven National Laboratory
Research Library
Attn: Reference Section
Upton, L. I. New York

Union Carbide Nuclear Company
Oak Ridge National Laboratory
Laboratory Records Department
P. O. Box P
Oak Ridge, Tenn.

Union Carbide Nuclear Company
Post Office Box P
K-25 Plant Records Department
Building K-1034
Oak Ridge, Tennessee

Office of Ordnance Research
U. S. Army
Box CM, Duke Station
Durham, North Carolina
Attn: Phys. Sciences Division

Commanding Officer and Director
U. S. Naval Radiological Defense Laboratory
Attn: Library Branch, Code 3-222A
San Francisco 24, California

Commander, U. S. Naval Ordnance Test Station
Code 753
China Lake, California

Commanding General
Air Force Cambridge Research Center
Attn: CROOTR
L. C. Hanscom Field
Bedford, Massachusetts

Professional

Dr. M. Pomerantz
Bartol Research Foundation
Franklin Institute
Whittier Place
Swarthmore, Pennsylvania

Professor C. D. Anderson
Norman Bridge Laboratory of Physics
California Institute of Technology
Pasadena 4, California

Professor W. A. Fowler
Kellogg Radiation Laboratory
California Institute of Technology
Pasadena 4, California

Professor W. B. Fretter
Department of Physics
University of California
Berkeley 4, California

Professor J. R. Richardson
Department of Physics
University of California
Los Angeles 24, California

Professor S. L. Glashow
University of California
Department of Physics
Berkeley, California

Professor M. Baranger
Department of Physics
Carnegie Institute of Tech.
Pittsburg, Pa.

Professor C. L. Cowan
Physics Department
Catholic University
Washington 17, D. C.

Professor H. L. Anderson
Department of Physics
University of Chicago
5801 Ellis Avenue
Chicago 37, Illinois

Professor J. Rainwater
Columbia University
Nevis Cyclotron Laboratories
P. O. Box 117
Irvington-on-Hudson, New York

Professor R. R. Wilson
Lab. of Nuclear Studies
Cornell University
Ithica, New York

Professor H. A. Bethe
Laboratory of Nuclear Studies
Cornell University
Ithaca, New York

Professor K. Wildermuth
Department of Physics
Florida State University
Tallahassee, Florida

Dr. R. B. Walton
General Atomic
Division of General Dynamics Corp.
P. O. Box 608
San Diego 12, California

Dr. R. B. Walton
General Atomic
Div. of General Dynamics Corp.
P. O. Box 608
San Diego 12, California

Professor R. W. Hickman
Department of Physics
Harvard University
Cambridge 38, Massachusetts

Professor F. Seitz
Department of Illinois
Urbana, Illinois

Professor A. C. G. Mitchell
Department of Physics
Indiana University
Bloomington, Indiana

Professor J. A. Van Allen
Department of Physics
State University of Iowa
Iowa City, Iowa

Professor H. Holmgren
Department of Physics and Astronomy
Maryland University
College Park, Maryland

Professor I. W. Jones
Department of Physics
University of Michigan
Ann Arbor, Michigan

Professor A. O. E. Nier
Department of Physics
University of Minnesota
Minneapolis 14, Minnesota

Professor E. P. Ney
Department of Physics
University of Minnesota
Minneapolis 14, Minnesota

Dr. M. J. Berger
National Bureau of Standards
Commerce Department
Washington 25, D. C.

Professor M. M. Block
Department of Physics
Northwestern University
Evanston, Illinois

Professor W. C. Miller
Nuclear Physics Laboratory
University of Notre Dame
Notre Dame, Indiana

Professor A. J. Allen
Department of Physics
University of Pittsbury
Pittsburgh 13, Pennsylvania

Professor G. Reynolds
Department of Physics
Princeton University
Princeton, New Jersey

Professor G. K. O'Neill
Princeton University
Department of Physics
Princeton, New Jersey

Professor Leon Katz
Linear Accelerator Lab.
University of Saskatchewan
Saskatoon, Canada

Professor W. E. Meyerhof
Department of Physics
Stanford University
Stanford, California

Professor W. C. Barber
Department of Physics
Stanford University
Stanford, California

Professor E. M. Harth
Syracuse University Research Institute
Syracuse 10, New York

Professor J. J. Lord
Department of Physics
University of Washington
Seattle 5, Washington

Professor J. Dreitlein
Department of Physics
Washington University
St. Louis, Missouri

Professor W. E. Stephens
Department of Physics
University of Pennsylvania
Philadelphia 4, Pennsylvania

Dr. P. T. Demos
Laboratory for Nuclear Science
MIT

Physics Library
c/o N. M. Hintz
School of Physics
University of Minnesota
Minneapolis 14, Minnesota

Foreign

Dr. Peter Brix
Institut F. Techn. Kernphysik
Technische Hochschule
Darmstadt, West Germany

Mme. O. Lebey
Service de Physique Corpusculaire
a Haute Energie
C. E. N. Saclay
B. P. No. 2
Gif-sur-Yvette (S. et O.)
France

Rutherford High Energy Laboratory
Harwell
Didcot, Berkshire
England

Professor Oscar Sala
Universidade de Sao Paulo
Faculdade de Filosophia
Ciencias e Letras
Caixa Postal 8 105
Sao Paulo, Brazil

Professor M. Conversi
Instituto di Fisica dell'Universita
P. le della Scienze, 5
Roma, Italy

Dr. Drik Smars
Royal Inst. of Tech.
Stockholm, Sweden

Prof. Denys Wilkinson
Cavendish Laboratory
Cambridge University
Free School Lane
Cambridge, England

Professor F. C. Chapman
Department of Physics
University of London
King's College
Strand, London, W. C. 2
England

Scientific Information Service
Attn: Mrs. L. Goldschmidt Clermont
CERN
Geneva 23, Switzerland

Professor L. A. Radicati
Universita di Pisa
Insituto di Fisica
Pisa, Italy

Professor J. L. Verhaeghe
Linear Accelerator Laboratory
University of Ghent
Coupure
Ghent, Belgium

J. L. Delcroix
Ecole Normale Superieure
Laboratoire de Physique
24 Rue L'Homond
Paris 5, France

Dr. B. Milman
Laboratoire des Hautes Energies
B. P. No. 2
Orsay (S. et O.)
France

Library
Institute for Nuclear Study
University of Tokyo
Tanashi-Machi, Kitatama-Gun
Tokyo, Japan